
Solar oscillations and helioseismology

Lidia van Driel-Gesztelyi

lvdg@mssl.ucl.ac.uk

<http://mssl.ucl.ac.uk/~lvdg/teaching.html>

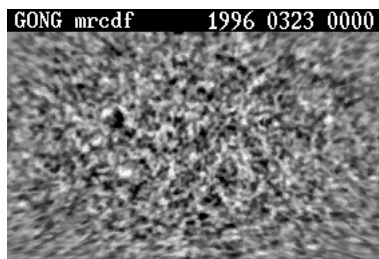
Introduction

- The internal layers of the Sun are not directly accessible to observations.
- However, it is possible to construct a **plausible picture of the interior** with the help of mathematical equations considering **mechanical and thermal equilibrium**, with boundary conditions provided by observations ⇒ **Standard Solar Model (SSM)**.
- The SSM use many approximations (no rotation, no magnetic field) to capture the essential characteristics of the Sun with minimum complication.
- Despite their shortcomings, models of the Sun are extremely successful and triumphs of 20th century solar physics and astrophysics.
- How can we test and improve the SSM?

Solar oscillations

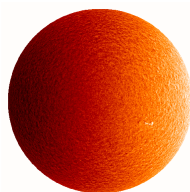
The **standard solar model** can be tested by

- neutrino measurements
- solar oscillations



one network day (24^h) of GONG p-mode images from March 23, 1996

Helioseismology

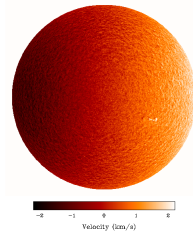


SDO/HMI
 Partial Localized Oscillation for Solar Oscillations

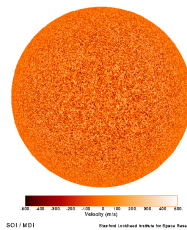
- Small amplitude/low frequency **oscillations** detected at the surface provide evidence of **seismic activity** in the interior.
- Detailed study of these oscillations provides information about the **Sun's internal structure** just as seismology provides details of the internal structure of the Earth
- Hence the title of the recently established subject: HELIOSEISMOLOGY (Deubner & Gough, 1984).
- For the **Earth**, we usually have one source of agitation: **earthquake**. For the **Sun**, not one source generates solar 'seismic' waves. The sources of agitation causing the solar waves that we observe are **processes in the larger convective region**.

Discovery of oscillations

- Oscillatory motions on the Sun were **first reported in Doppler imaging** observations of the solar photosphere by Leighton, Noyes & Simon in 1960. They measured small **displacements in the wavelength** of atmospheric absorption lines alternating between towards and away from the observer.

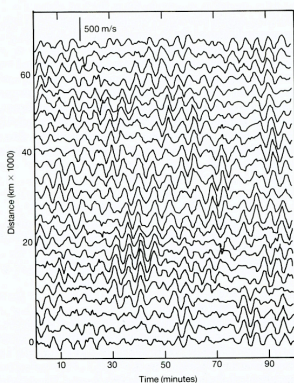


MDI single Dopplergram.
Note the effect of the solar rotation:
towards us - dark; away from us - lighter



Single Dopplergram - 45-image average
reveals the oscillatory surface motions

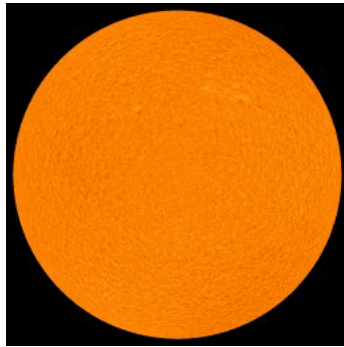
5-min oscillations



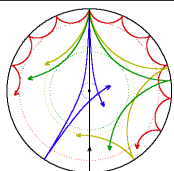
Howard, Tanerbaum & Wilcox, 1968

- Quasi-sinusoidal velocity profile
amplitude of hundreds of m s^{-1}
period of around **5 min.**;
the same pattern persists for $\sim 0.5^{\text{h}}$ (~ 6 wave cycles)
- Increased modulation at disc centre \Rightarrow
~ radial oscillations
- The amplitude increases only slightly with height
in the atmosphere and there is very little phase
difference between oscillations measured at
different height \Rightarrow **standing waves**
- Oscillations can also be detected as small
intensity variations.

Another movie (full-disc)

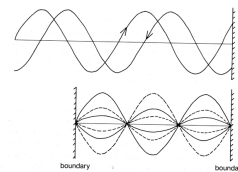


Note that oscillations are best observable in the central part of the Sun
 → radial oscillations



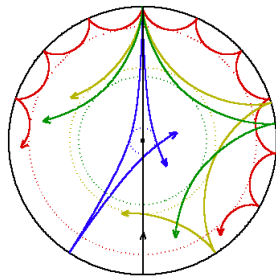
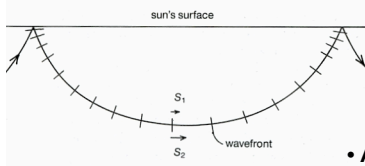
What is the cause?

- Ulrich (1970) and, independently, Leibacher & Stein (1971) proposed that the **oscillations are due to standing acoustic waves trapped in cavities** that extend well into the Sun.



- **Convection could excite such stationary sound waves**, which would be reflected from two boundaries and establish a variety of modes.
- Restoring force for sound waves is gas pressure. They can be reflected from boundaries, forming an acoustic cavity in which waves travel repeatedly. At the two boundaries nodes (with zero displacement) are established. Many standing wave modes can exist between nodes.
- Solar analogue of these wave modes: **p-modes** (p stands for pressure).

Ray paths



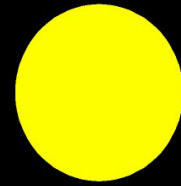
Shallower the angle, shallower its penetration depth - higher angle (\rightarrow longer λ), deeper penetration depth

- Acoustic cavities can exist without solid boundaries, e.g. in the solar interior.

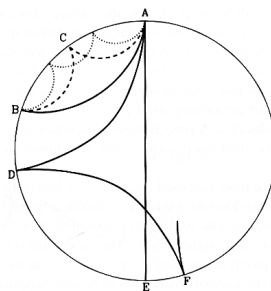
- T is increasing steeply towards the centre, so does the sound speed: $v_s \propto (T)^{1/2}$.

- Thus for a sound wave, which propagates towards the interior from the surface at an angle, the wavefront's (perpendicular to the direction of the wave) deeper edge travels faster than its upper edge \Rightarrow the wave turns gradually and will travel in an arc. **The wave undergoes total internal refraction.**

- *Solar acoustic cavity (spherical shell):*
Sun's surface (sharp ρ gradient) + base of each arc.



Wave interaction



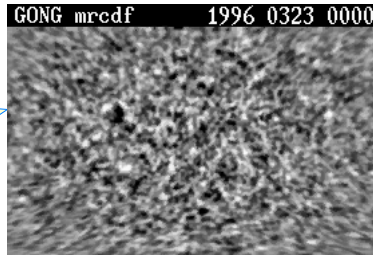
Consider two waves leaving A and arriving at B in phase.

An oscillation will be seen provided the paths differ by an exact number of wavelengths, the waves reinforce and become strong. Otherwise they interfere and are of negligible amplitude.

Observations - a movie

Solar oscillations may be regarded as a superposition of many standing waves.

one network day of GONG p-mode images from March 23, 1996



Produced by: Brian Pohl, Jim Pintar and David Jaksha

1440 frames (one 24-hour day)

P- and g- and f-mode waves

- Small departures from hydrostatic equilibrium caused by
 - turbulent convection
 - localized events related to solar activity (e.g. flares)

- Restoring force \Rightarrow oscillations \Rightarrow waves.
Self-interference \Rightarrow global normal modes.

- Small departures $a = a_0 + a'$ can be treated linearly: $\rho_0 \frac{\partial \bar{v}}{\partial t} = -\nabla P' + \rho' \bar{g}$

\Rightarrow Restoring forces:

- pressure gradient $-\nabla P' \Rightarrow$ **sound waves** (longitudinal, isotropic) \rightarrow p-modes (high-v)
- buoyancy $\rho' g \Rightarrow$ **gravity waves** (transversal, horizontal)
 - surface gravity waves** (ρ_0 discontinuous) \rightarrow f-mode (no compression)
 - internal gravity waves** (ρ_0 continuous) \rightarrow g-modes (low-v)

- Fundamental (f-) modes are without compression, it is like a surface wave on deep water.
- P-modes reach high amplitudes in the outer regions of the star, while g-modes in its inner part.

Excitation and damping mechanism

P-modes are stochastically excited and intrinsically damped by the convection. The stochastic excitation mechanism limits the amplitudes of the p modes to intrinsically weak values.

Excitation

- **P-mode** oscillations can be excited through stochastic generation of acoustic noise by convective zone motions. \Rightarrow intermittent process.
- Sources:
 - fluctuating turbulent pressure (Reynolds stresses)
 - fluctuating gas pressure
- **G-modes** in the solar core may be excited by nuclear burning instabilities.

Damping

- Damping mechanism is required to limit the amplitude of the oscillations.
 - radiative losses
 - viscosity
 - non-linear interactions between modes
- The amplitude of a mode is determined by a balance between excitation in some region of the solar interior and damping over a (different) volume of the solar interior.
- For low-l p-modes exponential decay with an e-folding time of several days were found. observations also suggest intermittent excitations of such global waves every few days.

Ridges of p and f modes

- **Power is not evenly distributed in the k_h , ω or λ_h , ν plane,** but follows certain **ridges**.

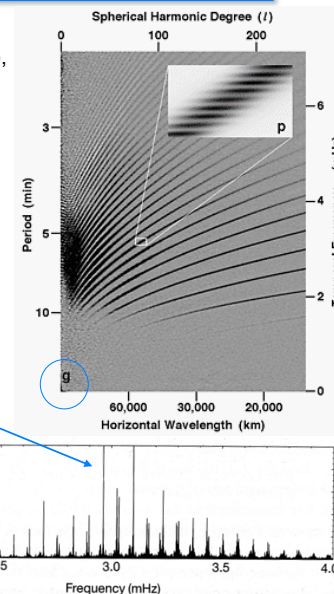
k_h : wave number ($2\pi/\lambda_h$) ω : angular frequency (rad s^{-1})
 λ_h : horizontal wavelength, ν : temporal frequency (Hz)
 l : harmonic (angular) degree
 \sim circumference/horizontal wavelength $2\pi R_\odot/\lambda_h$

- Ridges were theoretically predicted by Ulrich (1970) and first observed by Deubner (1975).

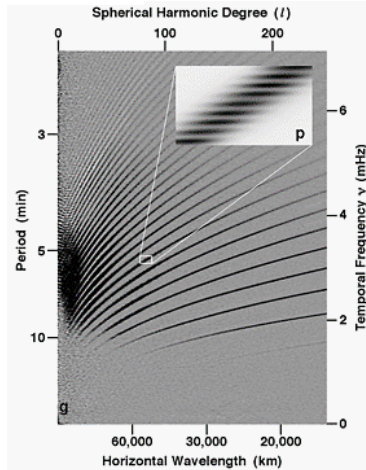
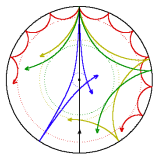
- **Most of the oscillatory power is between 2.5-4.5 mHz and $k_h < 0.8 \text{ Mm}^{-1}$, ($\lambda_h > 8 \cdot 10^3 \text{ km}$), $10 < l < 200$ period range: 4.8-6.5 min \Rightarrow 5-min oscillation.**

Due to the waves' long lifetime, destructive interference filters out all but the resonant frequencies, transforming the random convective noise into a very rich line spectrum in the five-minute range.

g-mode: $\nu \leq 0.3 \text{ mHz}$; ($T \geq 50 \text{ min}$)



Mode structure

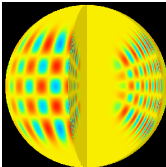


- Only waves with **specific combinations of period and horizontal wavelength resonate** within the Sun. The precise combinations are related to the **Sun's interior structure**; they produce the fine-tuned "ridges" of greater power.

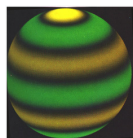
- Each of these modes is **trapped in a different region of the solar interior** and hence it is sensitive to structures and dynamics in the corresponding region.

- Combining information from these large number of independent modes it is possible to **infer the structure and dynamics of the solar interior** to unprecedented precision.

Quantum numbers

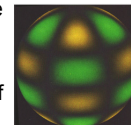


$l=20, m=16, n=14$



$l=6, m=0$

polar sensitivity



$l=6, m=3$

- Since the Sun is a spherical oscillator, the **p modes can be described in terms of spherical harmonics** by three quantum numbers: l , m & n .

- The **radial order**, given by n , is the number of nodes in the radial direction.

The order n tells how many times the pattern reverses itself inside the Sun between the surface and center. *The ridges in the l - ν diagram correspond to modes of different radial order n .*

- The **harmonic or angular degree**, called l indicates the number of node lines on the surface, which is the *total* number of planes slicing through the Sun. $l=0$ is the "radial mode".

- The **azimuthal number (order)**, m , tells how many of the surface nodal lines cross the equator and also gives the phase; m describes the number of planes slicing through the Sun longitudinally.

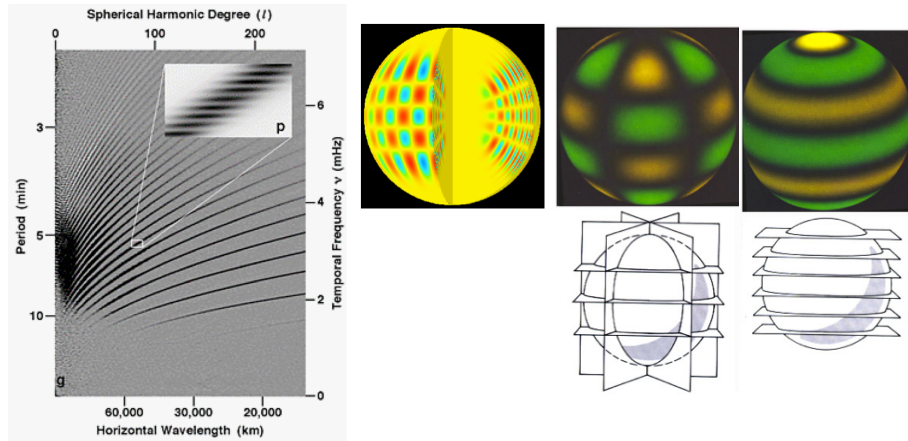
- In case of perfect spherical symmetry frequencies would be independent of m , but due to rotation, magnetic field and other possible (small) aspherical perturbations the frequencies depend on m .

In the presence of rotation, modes of the same n, l but different m are split into $2l+1$ frequency components due to their differing spatial oscillation patterns relative to the Sun's rotation axis. ($-l \leq m \leq +l$)

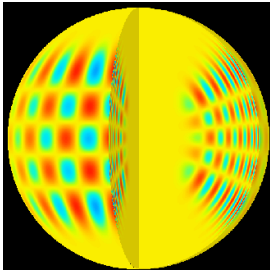
Global modes

Global modes: $a_{lm}(\omega)$ has sharp peak at certain values $\omega_{nlm} = \omega_n(l, m) = \omega_n(l)$.

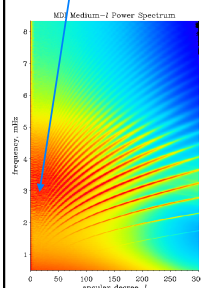
Spherical symmetry



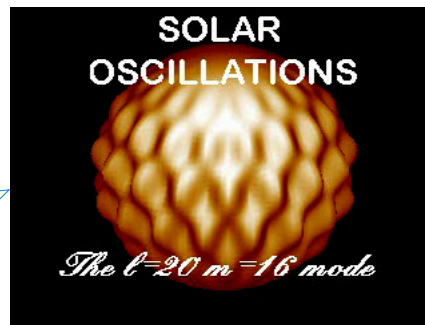
P-mode movie - model



$l=20, m=16, n=14$
 $\nu=2.93588 \pm 0.00002$ mHz



$l=20, m=16$ oscillation mode: prograde, retrograde, and standing waves

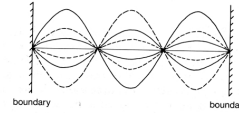


Produced by: David H. Hathaway. (NASA/MSFC)

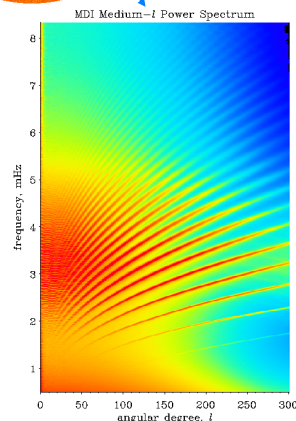
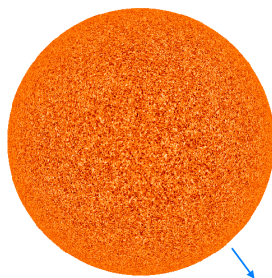
This is just one mode. However, the number of possible modes is high: $\approx 10^6 - 10^7$.
Solar oscillations may be regarded as a superposition of many standing waves.

Effect of solar rotation

- A standing wave arises from two waves traveling in opposite directions between two nodes. Their frequencies will be identical if there is no rotation.



- But with rotation the waves are carried in opposite directions at the rotation velocity v . So the **wave moving in the sense of the rotation** will have its frequency Doppler shifted by $\frac{\Delta\omega_+}{\omega} = \frac{v_+}{v_p}$ where v_p is the wave's phase velocity.
- The **oppositely directed wave** will undergo a reduction of $\Delta\omega$. I.e.: $\frac{\Delta\omega_-}{\omega} = \frac{v_-}{v_p}$
- Hence the **two waves** will be separated or **split** in frequency by $2\Delta\omega$.
- Overall, at the surface, this results in the entire standing wave pattern drifting slowly across the Sun in the opposite direction to that of the solar rotation.



Data reduction

- Images (observed $a'(\theta, \phi, t)$) are first decomposed into spatial spherical harmonics

$$a' = \sum_{lm} a_{lm}(t) Y_l^m(\theta, \phi)$$

where θ is the colatitude and ϕ is the longitude.

- The amplitude $a_{lm}(t)$ contains all modes with l, m values \rightarrow **Fourier transform** of $a_{lm}(t)$ gives the frequencies of oscillations of all these modes. $a_{lm}(t)$ is Fourier decomposed into $a_{lm}(\omega)$.

- The final result is a power spectrum of three variables: ν , l and m .

- The frequencies of modes with different values of m but same values of l and n are nearly degenerate. \Rightarrow for many purposes m -dependent frequency splitting is determined and then removed.

- The frequency-corrected spectra are then averaged over the range of m states to produce the $l - \nu$ spectrum shown in the figure.

Observational limits

Rule: a signal of length T allows a frequency resolution of $\Delta\omega=2\pi/T$ to resolve neighbouring frequencies ω and $\omega+\Delta\omega$, we must observe for $T=2\pi/\Delta\omega$ after which the two oscillations acquire a phase difference of 2π .

The lowest ω visible in the signal is determined by T , and is equal to the frequency resolution.

After one day of observation the frequency resolution is $\nu=1/T \sim 1.16 \times 10^{-5}$ Hz (11.6 μ Hz).

After about ten years, the frequency resolution is $\nu=1/T \sim 3.18 \times 10^{-9}$ Hz (3.18 nHz).

The high frequency limit is given by the time resolution Δt of the data.

$\omega_{Ny}=\pi/\Delta t$ - Nyquist frequency - $\omega > \omega_{Ny}$ should be suppressed in the data.

Summary: $\Delta\omega = 2\pi/T \leq \omega \leq \pi/\Delta t$ (since $\omega = 2\pi\nu$, thus $\Delta\nu = 1/T \leq \nu \leq 1/(2\Delta t)$)

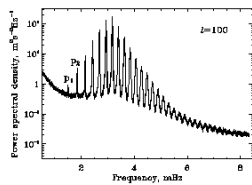
Since SOHO/MDI observes every 60 seconds, the high-frequency limit in the data is $1/(2\Delta t) = 1/120=8.3 \times 10^{-3}$ Hz (8.3 mHz)

The same is true for space and wave domains, hence the largest possible k is limited by the sampling process:

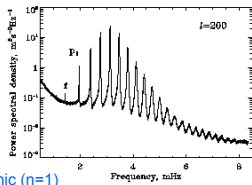
$$\Delta k_x = 2\pi/L_x \leq k_x \leq \pi/\Delta x \quad (\text{since } k=2\pi/\lambda, \Delta\lambda_x = 2\Delta x \leq \lambda_x \leq L_x)$$

Where L_x the length of a scan in x direction with spacing Δx and k_x is the x component of the wave vector. The Nyquist wave number $k_{Ny} \leq \pi/\Delta x$ (or $\lambda_{Ny} \geq 2\Delta x$).

P-mode ridges



MDI Power Spectra
Vertical slices at $l = 100, 200,$ and 300 from the data of the right-hand figure. Note the low noise levels and the clear power peaks up to the Nyquist frequency $\omega_{Ny}=\pi/\Delta t$; $\nu_{Ny}=1/(2\Delta t)$. $\nu_{Ny} \sim 1/(2\Delta t) = 1/120=8.3 \cdot 10^{-3}$ Hz (8.3 mHz)

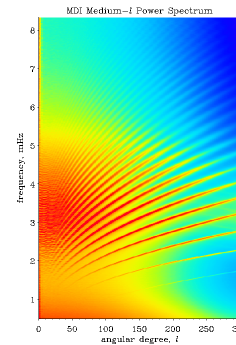


The ridges in the l - ν diagram correspond to modes of different radial order n .

For the same l , each peak (ridge) represents a mode with different number of nodes in the radial direction (different n) - higher the frequency, higher the number of radial nodes \Rightarrow for a given $l \neq 0$ the depth of penetration increases with frequency.

1st harmonic ($n=1$)

fundamental (surface) mode ($n=0$)



Observational requirements

- For a typical visible solar spectrum line: $\lambda = 600 \text{ nm}$ and width $\approx 10 \text{ pm}$, then a $v = 1 \text{ m s}^{-1}$ shifts the line about 0.002 pm .
- In helioseismology, some individual oscillation modes have amplitudes of no more than about 0.1 m s^{-1} . Goal is to measure shifts of a spectrum line to an accuracy of 10^{-6} of its width...
- The Doppler velocity amplitudes are $\pm 0.5 \text{ km s}^{-1}$ maximum and extend down to the $\pm 0.1 \text{ m s}^{-1}$ level for the low degree modes. These small velocities are measured with high resolution Michelson interferometers or with specialised resonance absorption gas cells placed in a magnetic field.
Detection of the brightness oscillations requires extremely sensitive photometry.
- The critical measurement in helioseismology is the precise frequency of each mode of interest. The more cycles one observes the more precise the result.
- Lifetimes of the modes can be quite long, up to many months.
Making good measurements means making very long observations.

The effect of interruptions

There is an obvious problem with making uninterrupted observations from a single earth-based site. Such **observations** from anywhere except within the arctic or Antarctic circles will be **chopped by the day/night cycle**.

This leads to a **time series that is the product of a nominal square-wave window function and the essentially sinusoidal solar oscillations**. The resulting spectrum consists of each true solar line surrounded by a forest of artifactual sidelobes corresponding to the harmonics of the 1/day chopping frequency. This **complex sidelobe structure** is quite dense and can make it very difficult to distinguish between the solar signals and the artifacts.

Moreover, even aperiodic interruptions raise the general background noise level when the time series is transformed into frequency space.

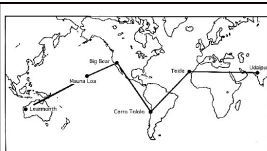
$$\nu_{\text{lobe}} = 1/T = 1/86400\text{s} = 11.57 \mu\text{Hz}, \text{ relative power} \sim \text{relative length of obs/break}$$

Observing venues

Ideal helioseismology observations are uninterrupted and last for years.

Alternative venues:

- unclipped instrument in space
- observatories at the Earth's poles
- network of observatories around the Earth



Observing programs - ground-based

BISON (Birmingham Solar Oscillations Network): developed by the University of Birmingham. They do **Doppler velocity** measurements using optical spectrum lines **in the Sun's integrated light**. The network includes six observatories in California, Tenerife, Chile, S. Africa and E & W Australia.

IRIS (International Research on the Interior of the Sun): developed by the University of Nice. Sites include the Antarctic, Chile, California, Marocco. They also **observe the integrated radial velocity of the Sun**.

BiSON and IRIS are probing mainly deep solar layers..

GONG (Global Oscillations Network Group) involves 6 ground based Observatories (in California, Hawaii, Australia, India, Tenerife, Chile). GONG consists of 67 collaborating institutes from all around the world. GONG has been making **spatially resolved Doppler measurements** of the Sun since October 1995.

TON (Taiwan Oscillation Network) measures intensity oscillations in the Ca II K line.

Observing venues - SOHO

The joint ESA/NASA **SOHO** spacecraft launched in 1995 December, is observing in constant sunlight near the Earth-Sun L1 Lagrangian point. It is another great advantage that the spacecraft has a very low velocity relative to the Sun.

SOHO carries three helioseismic experiments:

- (i) **SO/MDI** (Solar Oscillations Investigation/Michelson Doppler Imager)– Investigates the line-of-sight surface **velocity field**.
- (ii) **GOLF** (Global Oscillations at Low Frequencies) – detection of **global** oscillations in the 10^{-7} - 10^{-2} Hz frequency range, with emphasis on the low order, long period waves which penetrate the solar core - **velocity field** observations.
- (iii) **VIRGO** (Variability of solar IRradiance and Gravity Oscillations) - measurements of solar total and **spectral irradiance** and its variations, attempt (unsuccessful so far) to detect low-degree g-mode oscillations.

Calculating physical quantities

Given an **equilibrium solar model** we calculate frequencies considering **small perturbations** about the equilibrium structure. The equilibrium model is spherically symmetric, perturbations can be expressed in terms of the **spherical harmonics** $Y_{lm}(\theta, \phi)$. E.g. the pressure can be written as:

$$p(r, \theta, \phi, t) = p_0(r) + \sum_{n,l,m} A_{nlm} R_{nlm}(r) Y_{lm}(\theta, \phi) e^{-i\omega_{nlm} t}$$

where r is the radial distance from the centre, θ the colatitude, ϕ the longitude, n, l, m are the quantum numbers specifying the eigenmode of oscillations, ω_{nlm} is the frequency of the corresponding mode, $R_{n,l,m}(r)$ defines the radial dependence of the eigenfunction, and $p_0(r)$ is the pressure profile in the equilibrium solar model.

Similarly, all other scalar quantities can be calculated.

T of oscillations \ll **thermal time-scale** (10^6 ys in the core \rightarrow few minutes in the photosphere) they can be treated as **adiabatic** in the interior of the Sun, but not so close to the surface - the latter non-adiabatic effects (e.g. convection) are not treated well presently.

Probing the solar interior

Helioseismic data of oscillation frequencies may be analysed in two ways:

- forward method
- inverse method - global oscillations (infer global mean structure)
 - local area helioseismology (explore local/temporary internal structures)

In the **forward method** a set of solar models are constructed using the structure equations with different values of adjustable parameters. The equilibrium model is then perturbed using a linearised theory to obtain the eigenfrequencies of solar oscillations. The fit between the theoretically computed and measured frequencies never turns out to be perfect and the correlations between different parameters make it difficult to determine these parameters uniquely.

Alternately, we can use **inversion techniques** to calculate the internal structure of the Sun directly from the observed frequencies. Although these inversion techniques generally require a reference solar model to calculate the sound speed and density profiles inside the Sun, the inferred profiles are not particularly sensitive to the choice of the reference model.

“Local area” helioseismology investigates local properties of solar oscillations.

Helioseismology - direct modeling (1)

Direct modelling

- computation of a solar model using the basic equations
- calculation of r -dependent coefficients of the oscillation equations
- solve these equations numerically, with appropriate boundary conditions
- ⇒ eigenfunctions $P_1(r)$...
- ⇒ eigenfrequencies: particular ω values for which non-zero solution exists
(more widely used)

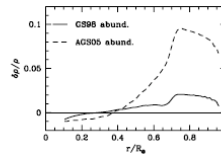
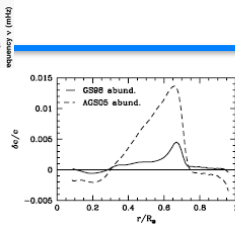
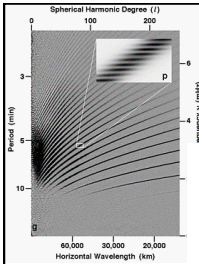
The standard solar model (SSM) contains uncertainties (deviations from the perfect gas law, precise value of Z , fractional abundance of heavier elements)

- ⇒ vary these to bring the calculated eigenfrequencies closer to the observed ones
- ⇒ the “best solar model”

Calculate the model eigenfrequencies with precision of the observed ones...

Sometimes comparison of frequency differences is sufficient.

Direct modeling (2)



Relative sound-speed (δ) and density difference (r) between the Sun and a standard model constructed with High-Z (1.018; dashed) and low-Z (0.012; full) metallicity. (Chaplin and Basu, 2008)

• Chemical composition

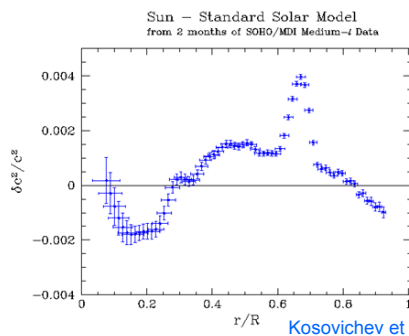
Direct modeling forced modelers to reject the low-Z SSM, which was designed to remove the solar neutrino problem due to its lower opacity & temperature in the solar core. **Note: low-Z models have much shallower convection zone of the Sun.** $Z = 0.001, 0.004$ didn't work, only $Z = 0.02$ gave satisfactory agreement between calculated eigenfrequencies and observed frequencies (Christensen-Dalsgaard & Gough, 1981).

$Z > 0.02$ would aggravate the neutrino problem and contradict the heavy element abundance determined spectroscopically.

• Equation of state

Electrostatic correction to the perfect gas law was needed - this became part of the SMM.

Inverse modeling result on $c(r)$ (1)



Relative differences between the sound speed v_s^2 (c^2) in the Sun, deduced from helioseismology observations, and in a recently computed SSM.

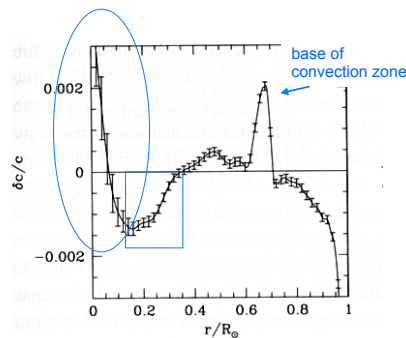
Note that the maximum difference in v_s^2 between the SSM and the Sun is only 0.4%.

$$v_s = c = \sqrt{\frac{\Gamma_1 P}{\rho}} \quad \text{where} \quad \Gamma_1 = \left(\frac{\partial \ln P}{\partial \ln \rho} \right)_s \quad \text{is the adiabatic index.}$$

- The **narrow peak at $0.67 R_\odot$** , just beneath the convection zone has been identified to be due to a **sharp gradient in the helium abundance profile in the solar model**. A moderate amount of **turbulent mixing** (due to rotationally induced instability) can solve the problem. This region is called the **tachocline**, where strong **rotational shear** was discovered, which is likely to induce the required mixing.

Inverse modeling result on $c(r)$ (2)

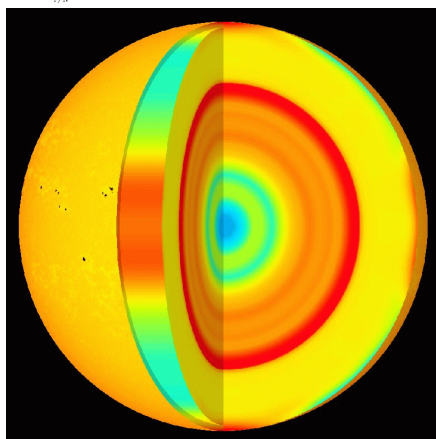
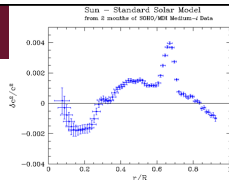
- The sharp decrease of the sound speed compared to the model at the boundary of the core at $0.25 R_{\odot}$ may indicate an over-abundance of helium at the edge of the energy-generating core.
- The steep increase of the sound speed towards the centre can be understood if the He is less abundant, i.e. it has a more flat abundance profile in the core than in the SSM, possibly due to use of incorrect nuclear reaction rates.
- Or may be the result of macroscopic motions in the core induced by the instability of ${}^3\text{He}$ burning.



Relative difference in the sound speed profile in the Sun, and a standard solar model. The steep drop near the surface is due to uncertainties of outer layers in the SSM.

Christensen-Dalsgaard et al, 1996

Inverse modeling result on $c(r)$ (3)



The sound speed in the solar interior as deduced from SOHO/MDI data **relative to** the one predicted by the SSM.

Red: **faster**, blue: **slower**

Recall that the sound speed is $c \propto T^{1/2}$, therefore this image tells us about the difference between the observed and modelled radial temperature profiles in the solar interior.

Uncertainties close to the surface:

- (1) Treatment of convection
- (2) Radiative transfer in the atmosphere
- (3) Non-adiabatic effects in the sub-surface layers.

The W(r) function

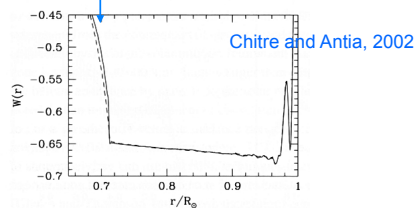
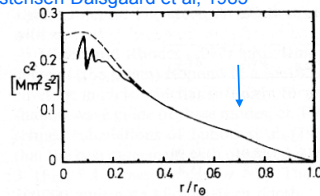
Study of $c(r)$ allows **depth of the convection zone** to be determined. Simple plot of c versus r won't do it (see figure left below).

However, the quantity $W(r)$ proves very useful: $W(r) = \frac{r^2}{GM_\odot} \frac{dc^2}{dr}$ where M is mass inside r

The *plot on the right* shows a sharp rise at the base of the convection zone at $r=0.713\pm 0.003 R_\odot$. In the **convection zone $W \sim -2/3$** , and is held constant due to hydrostatic adiabatic equilibrium.

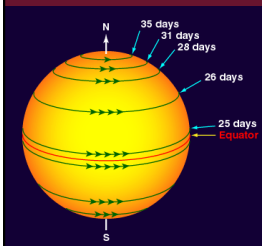
The sound speed ($c=\sqrt{\Gamma_1 P/\rho}$) profile in ionisation zones is affected by the variation of the adiabatic index, Γ_1 ($=\partial \ln P/\partial \ln \rho$)_S which in turn is determined by the chemical composition. The dip at $r=0.98 R_\odot$ in the figure is due to the dip in Γ_1 inside the He II ionisation zone. This peak can be calibrated to measure the helium abundance (Y) $\Rightarrow 0.249\pm 0.003$.

Christensen-Dalsgaard et al, 1985



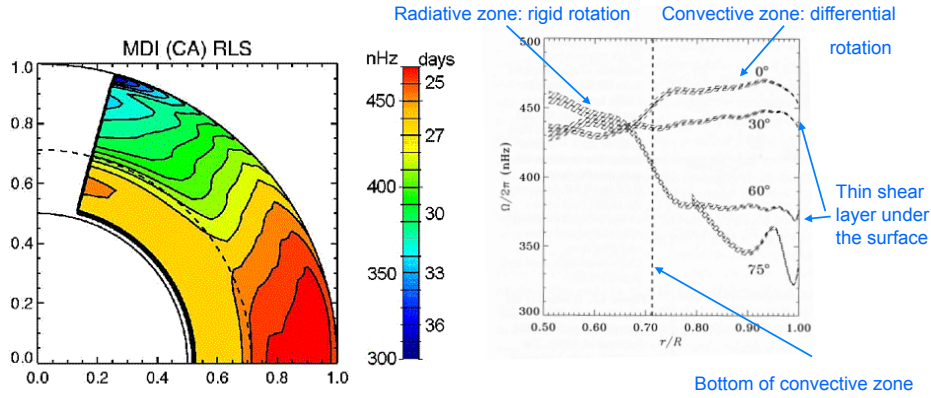
Note: the temperature gradient changes from adiabatic value inside the convection zone to radiative gradient below that \Rightarrow the discontinuity in the derivative of c^2 .

Inverse modeling - differential rotation



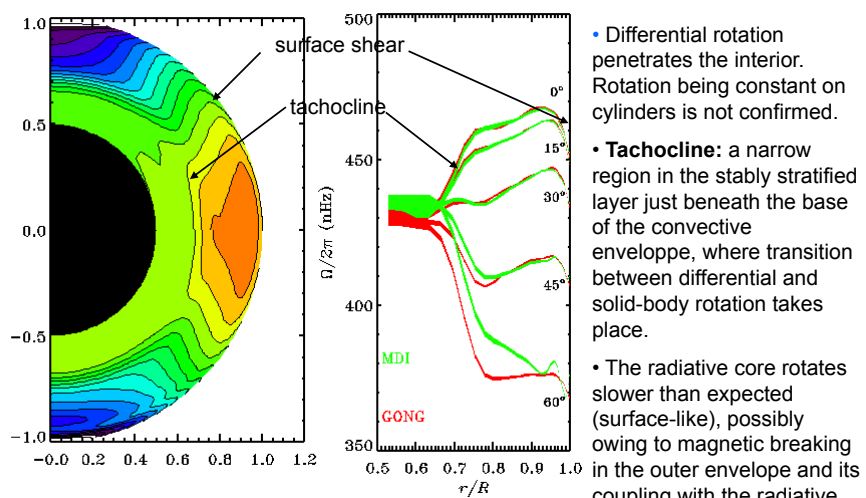
- In the Sun, angular velocity has a latitudinal dependence on the surface (differential rotation), so the depth dependence of the latitudinal shear should also be investigated.
- For an investigation of the full function $\Omega(r,\theta)$ the whole multiplet $2l+1$ should be used. The **deviation from equidistant spacing** within the multiplets is typical for latitudinal shear.
- **Method:** substitute a certain form of $\Omega(r,\theta)$ into the general expression for eigenfrequencies and compare the results with observed $\Delta\omega$ ($\Delta\nu$) values resulting from rotational splitting.
- **Result: down to the bottom of the convection zone latitudinal differential rotation is essentially the same as that of the surface** (along radial lines $\sim 27^\circ$ tilt to the rotation axis).

Inverse modeling - results on $\Omega(r,\theta)$



Time-averaged $\Omega(r,\theta)$ rotational profiles as deduced from inversions of data observed with SOHO/MDI.
 Red: fastest, blue: slowest. Note the sharp change under the surface.

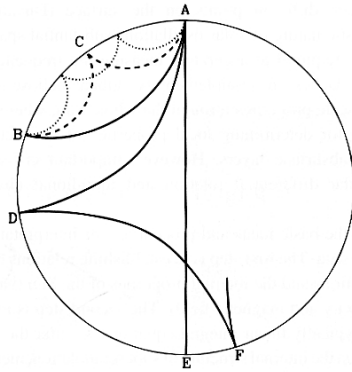
Global rotation profile



Comparison between results from GONG and MDI data (Howe, 2002)

- Differential rotation penetrates the interior. Rotation being constant on cylinders is not confirmed.
- **Tachocline:** a narrow region in the stably stratified layer just beneath the base of the convective envelope, where transition between differential and solid-body rotation takes place.
- The radiative core rotates slower than expected (surface-like), possibly owing to magnetic braking in the outer envelope and its coupling with the radiative core.

Inverse modeling - helioseismic tomography (1)



- Waves are excited at point A will re-appear at the surface points B... F propagating along ray paths reaching different depths.
- Because the sound speed is higher in deeper layers the direct waves arrive first, followed by the second-bounce and higher-bounce curves.

Inverse modeling - helioseismic tomography (2)

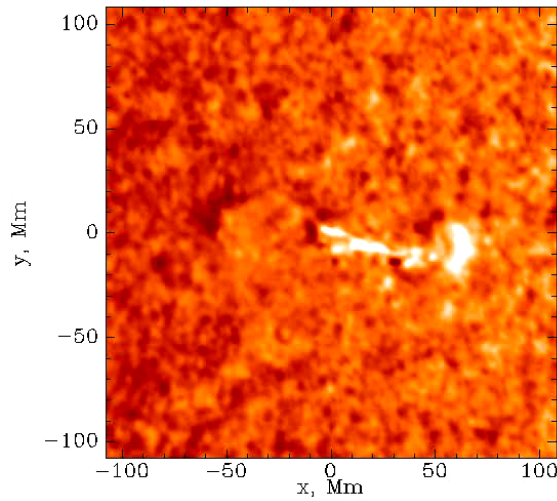
Helioseismic tomography probes **3-D structures and flows** beneath the solar surface. It belongs to the "local area" approach of helioseismology.

- (1) **The time for waves to travel** along subsurface ray paths is determined from the **temporal cross correlation** of signals at **two separated surface points**.
- (2) By measuring the times for **many pairs** of points from Dopplergrams covering the visible hemisphere information about the state of the solar interior is derived, e.g. properties of **convective** and **magnetic structures** in the surface layers.

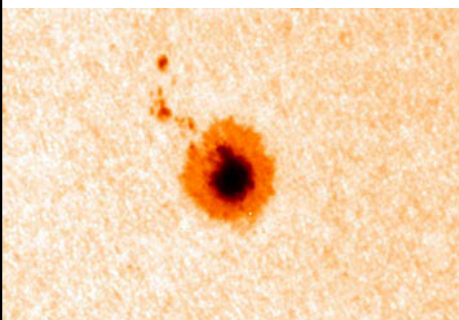
First step: **establish relations** between the observed **travel-time variations** and **internal properties** of the Sun (variations of the sound speed, flow velocity and magnetic field).

Second step: inversion of these relations, which are typically linear integral equations, to **infer the internal properties**.

Sunquakes – seismic effects of flares



Inverse modeling - time-distance



Sunspot data from MDI High Resolution, 18 June 1998

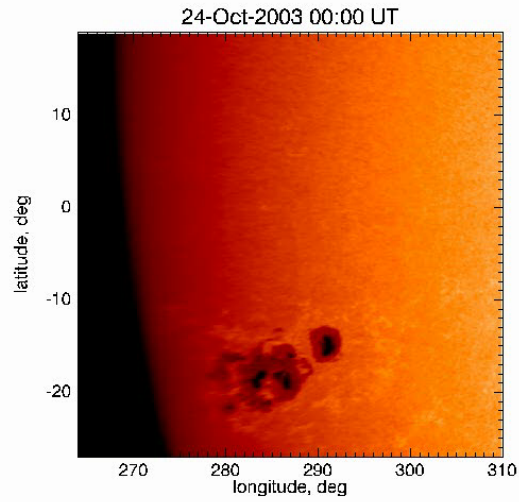
Time-distance methods provide a method to infer sound-speed variations and flows in the interior.

This view shows sound speed variations beneath a sunspot.

*The **sound speed is affected both by the temperature of the gas and the magnetic field**, which we know to be strong in the sunspot at the surface.*

The normal increase of sound speed with depth in the Sun has been subtracted so that we are only looking at deviations from the average.

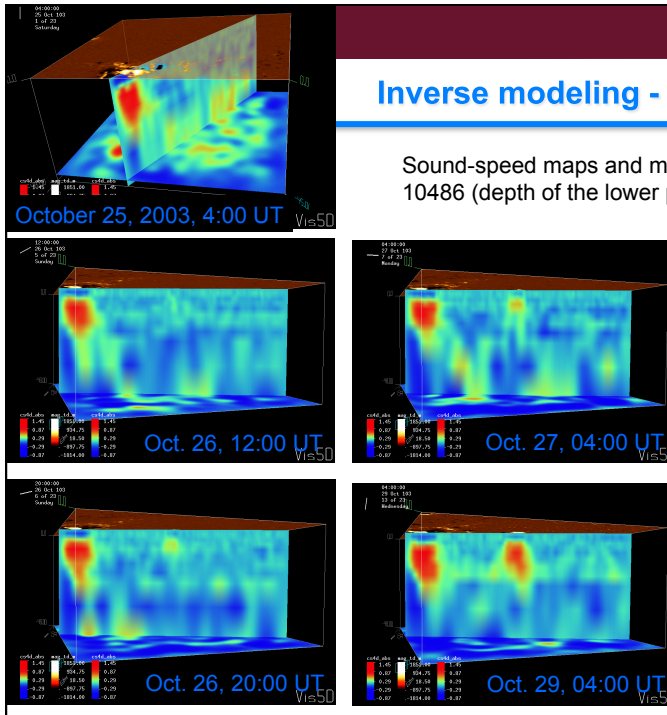
Inverse modelling - time-distance



Evolution of AR 10486-488: October 24 – November 2, 2003

Inverse modeling - time-distance

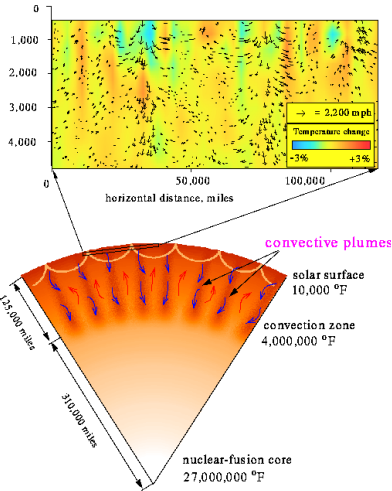
Sound-speed maps and magnetograms of AR 10486 (depth of the lower panels: 45 Mm)



Emerging magnetic field seen in time-distance data

Time-distance - interior dynamics

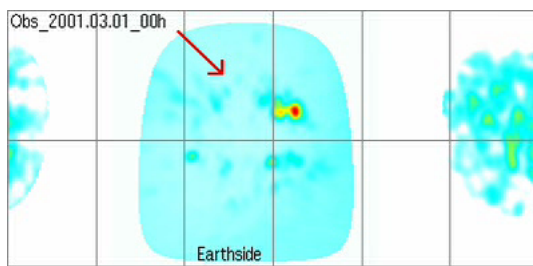
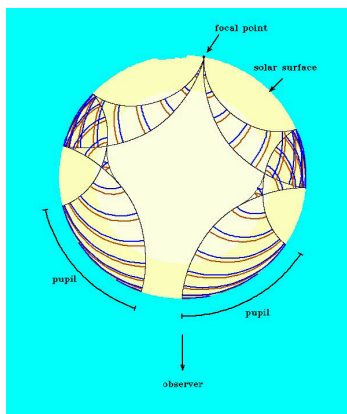
Convective Flows Below The Sun's Surface



This vertical slice shows a cross-section of **supergranulation**.

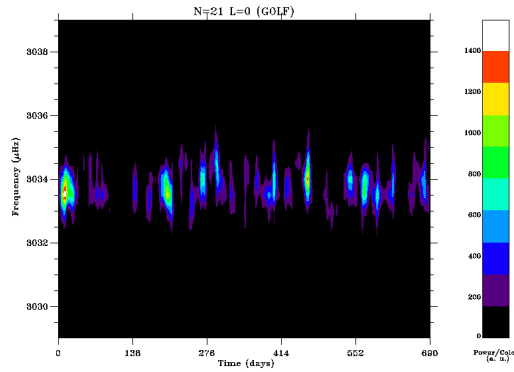
This analysis shows that **supergranulation extends something like 5-8 Mm into the interior vs. 20-30 Mm diameter**. Below this the supergranulation pattern disappears.

Far-side images of the Sun



Images of an active region on the **far side of the Sun** were derived by applying seismic holography to helioseismic observations.

Temporal changes - random



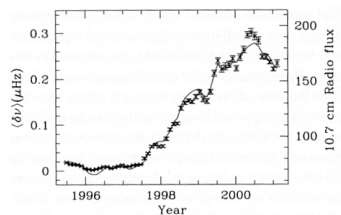
This time/frequency diagram shows the temporal behaviour of one of the p-modes. In the Fourier spectrum a **mode appears as a sharp peak in frequency**, but no information is available on its variations with time. **Time/frequency analysis** yields this information, and this figure illustrates the 'impulsive' behaviour of the power of the acoustic vibrations of the Sun, due to **their stochastic excitation** by the convection of the outermost layers of the solar interior.

Temporal changes - systematic

With SOHO and GONG data covering substantial part of the solar cycle (cycle 23), it has been possible to study temporal variations in the solar interior. It is found that **p-mode frequencies shift by up to 0.4 μHz during the solar cycle and that frequencies are larger during the solar maximum** (decrease 1 part in 10000 between cycle maximum and minimum).

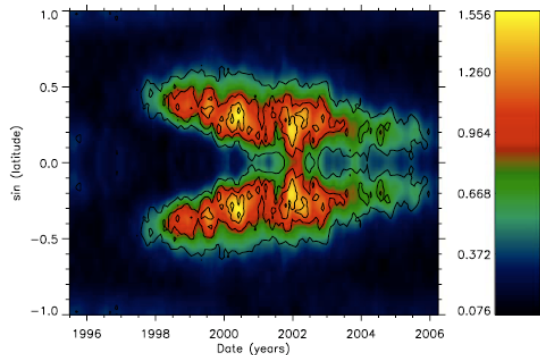
The frequency shift has a steep frequency dependence. Also, at the same frequency the deeper-penetrating modes show smaller frequency variations.

⇒ **The frequency variations are caused by perturbations in the outer(most) solar layers.**



The main frequency shift as a function of time in the GONG data. Over-plotted is the 10.7 cm radio flux, which is a well-used index of solar activity. The two datasets are well correlated.

Effect of surface activity

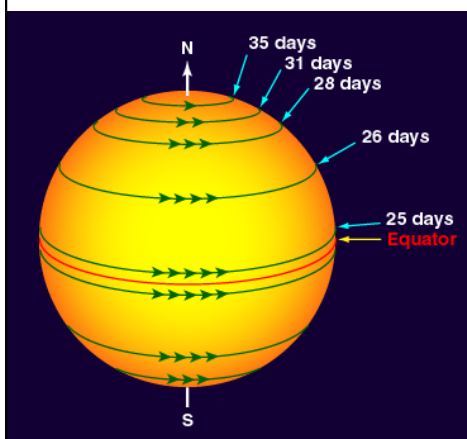


The mode frequency changes are owing to changes in the outer layers. The changes are associated with changing excitation and damping (e.g. power, damping rate...). Deep-penetrating flows indicate changes in the internal rotation rate.

Mode frequency shifts (in μHz) as a function of time and latitude (GONG result). The contour lines indicate surface magnetic activity, i.e. the presence of magnetic fields (L. Howe)

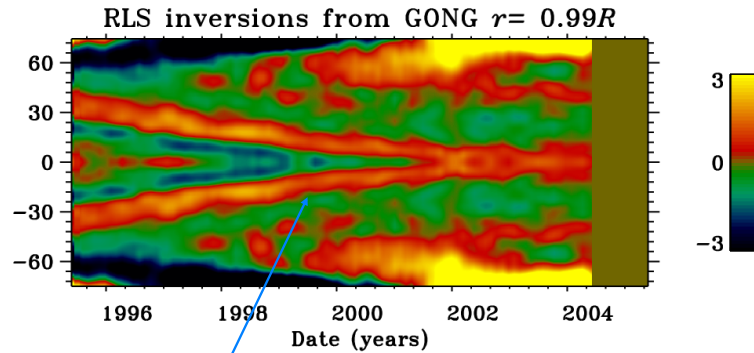
- The effects of magnetic field can be:
- **Direct:** Lorentz forces on the plasma provide another restoring force, resulting in an increase of frequency and the appearance of new modes.
 - **Indirect:** Magnetic fields can affect physical properties in the mode cavities.

Differential rotation



Temporal changes: torsional oscillations

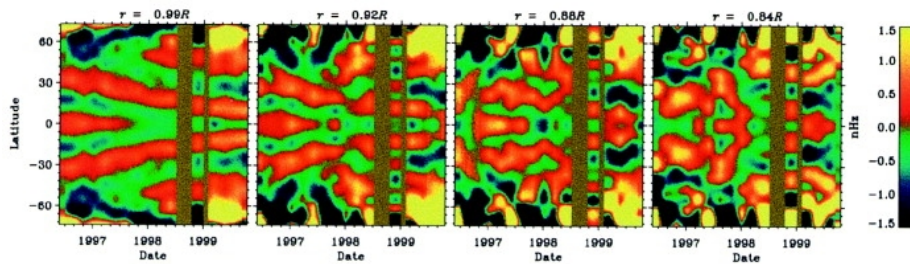
Changes of the differential rotation with the solar cycle - "torsional oscillations"
(rotation speed relative to mean speed)



Magnetic active regions appear at boundaries between fast and slow zones

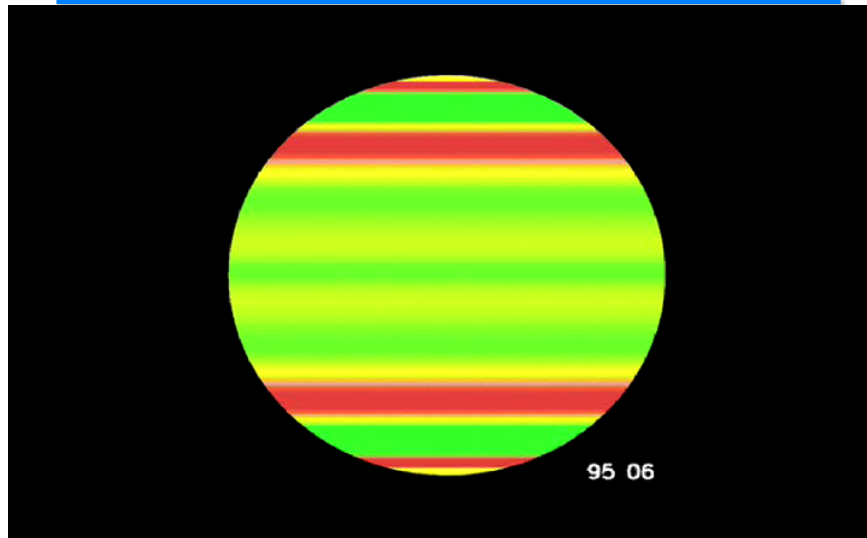
Temporal changes: torsional oscillations

The scale is in units of 1 nHz (this corresponds to 4 m/s at the equator).



Faster-than average rotational bands appear at the boundary of the activity zone. They extend to a depth of 1/3 of the convection zone from the surface. It appears that the magnetic field influences the distribution of the velocity field.

Temporal changes - the movie



Red, yellow: faster than average. Dark blue: slower than average

Summary

Small amplitude (0.1 m/s - 0.5 km/s) low frequency (2.5-4.5 mHz; ~5 min) oscillations are detected at the surface of the Sun in Doppler velocity and intensity measurements.

The oscillations are due to standing acoustic waves trapped in cavities that extend well into the Sun.

The p modes can be described in terms of spherical harmonics by three quantum numbers: l (harmonic or angular degree), m (azimuthal order) & n (radial order).

The basic idea of helioseismology:

Measure travel times τ or resonant frequencies ω (ν) of solar oscillations and to determine the internal properties of the Sun, such as the

- sound speed $c_s(r)$,
- density stratification,
- differential rotation
- mass flows